The Role of Precipitation on Bedrock Channel Incision in Kauai, HI

by

Michelle I. Slosberg

Submitted to the Department of Earth, Atmospheric and Planetary Sciences

in Partial Fulfillment of the Requirements for the Degree of

Bachelor of Science in Earth, Atmospheric and Planetary Sciences

at the Massachusetts Institute of Technology

February 2012

Author Signature redacted

Michelle I. Slosberg
Department of Earth, Atmospheric and Planetary Sciences
December 16, 2011

Certified by Signature redacted

Taylor Perron
Thesis Supervisor

Accepted by Signature redacted

Samuel Bowring
Chair, Committee on Undergraduate Program

The Role of Precipitation on Bedrock Channel Incision in Kauai, HI

by

Michelle I. Slosberg

Submitted to the Department of Earth, Atmospheric and Planetary Sciences

in Partial Fulfillment of the Requirements for the Degree of

Bachelor of Science in Earth, Atmospheric and Planetary Sciences

at the Massachusetts Institute of Technology

February 2012

Abstract

Erosion of bedrock channels is frequently modeled with the stream power law, which relates erosion rates to drainage area, slope, and an erosional efficiency coefficient k. The value of k, however, varies with many physical factors and most of these relationships are not well quantified. This study uses a form of stream power dependent on mean annual precipitation. The island of Kauai in the Hawaiian island chain is used as a case study due to the island's steep precipitation gradient and relatively constant lithology. Erosion rates are calculated by constructing splines to approximate the island's shape at the end of the shield-building phase, and these data are used to calculate erosion rates. The precipitation-dependent stream power model is tested with a multiple regression analysis of the Kauai data. Erosion rates are positively correlated with precipitation rates and erosional efficiency is related to precipitation rate by a power of ~0.4.

Supervisor: Taylor Perron

Title: Assistant Professor of Geology

Acknowledgements

I would like to sincerely thank Ken Ferrier for his countless hours of discussion and technical assistance throughout this project. I would also like to acknowledge Benjamin Black for providing ideas that inspired the basis for the initial spline fit code. Finally, thank you to my advisor, Taylor Perron, for his helpful insight and guidance.

Table of Contents

1 Introduction.....6

1.1 Stream Power Law.....7

1.2 Stream Power and Precipitation.....9

2 Methods.....10

2.1 Geology and topography of Kauai.....11

2.2 Climate.....14

2.3 Splines for estimating long-term erosion rates.....16

2.4 Topographic analysis to measure drainage area and slope.....22

3 Results.....23

4 Analysis and Discussion.....27

4.1 Erosion, erosional efficiency, and precipitation rates.....27

4.2 Exponent values.....29

4.3 Shear stress and stream power models.....29

4.4 Error and statistical significance.....31

4.5 Long- and short-term erosion rates.....31

5 Conclusions.....33

6 References.....35

7 Appendix: Geochronologic Measurements of Kauai Volcanic Flows.....39

List of Figures

Figure 1: Eight studies comparing erosion rates and average precipitation.....7

Figure 2: Map of Kauai.....12

Figure 3: Kauai geology and geochronology.....14

Figure 4: Mean annual precipitation as modeled by the PRISM climate model.....16

Figure 5: Example of spline fitting method for the Lumahai basin.....18

Figure 6: All spline surfaces for Kauai.....20

Figure 7: Erosion rate vs. basin-averaged mean annual precipitation.....24

Figure 8: Basin-averaged erosion rate vs. basin-averaged mean annual precipitation.....25

Figure 9: Precipitation-dependent erosional efficiency vs. basin-averaged mean annual precipitation.....26

List of Tables

Table 1: Basin geochronology.....22

Table 2: Mean erosion rates for each basin.....23

Table 3: Precipitation-dependent stream power exponents.....26

1 Introduction

Long-term erosional processes have a major impact on the topography of Earth. One of the main forces driving landscape evolution is bedrock river incision. Although even simple models of bedrock river incision depend on water discharge, which in turn should depend on rainfall rate, the connection has not been well quantified and the link between precipitation and erosion is not understood [Whipple 2004].

Studies conducted to investigate this relationship [e.g. Riebe et al. 2001] have shown little or no correlation between erosion rates and precipitation or climate. Of the studies that found correlation between erosion rates and precipitation rates, there is no overall agreement on the functional form of the relationship (Figure 1). Furthermore, in a review of these papers, Riebe et al. [2001] concluded that many of the studies that found correlation had statistically insignificant results. Despite these findings, it is still recognized that erosion rates should be linked to climate [Whipple 2004]. The lack of a clear relationship in these studies may be a consequence of analyses that used small datasets and had difficulty controlling for non-climatic variables that also effect erosion rates, which may obscure trends between erosion rates and precipitation rates. To overcome the problems faced by these studies, in this thesis I assemble a large dataset of erosion rates across a wide range of precipitation rates while controlling for major non-climatic variables such as rock type and tectonic context. Through this approach I was able to detect a signal in the data, indicating a positive correlation between erosion rate and precipitation rate and erosional efficiency and precipitation rate.

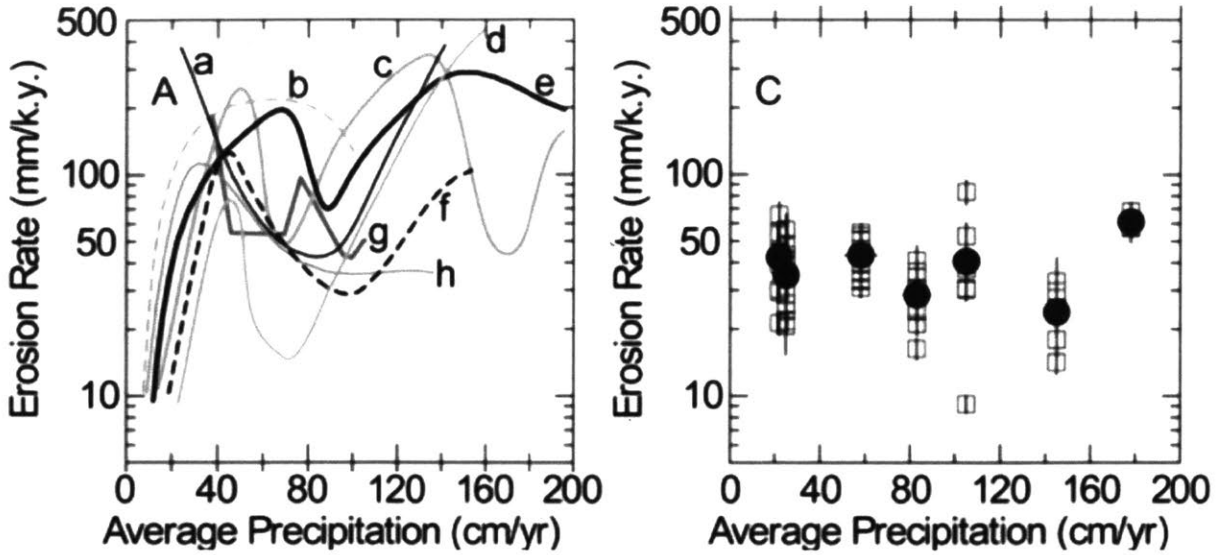

Figure 1: A. Eight studies comparing erosion rates and average precipitation. Each line represents data from a different study. These studies have not come to a clear consensus on the relationship between precipitation and erosion rate. C. Erosion rates from cosmogenic nuclide analysis. Again, no clear relationship is seen between erosion rate and average precipitation [Modified from Riebe et al. 2001].

1.1 Stream Power Law

The stream power law is a relationship commonly used to model erosion in bedrock by relating bedrock incision to physical properties of a channel. In this section, the stream power law will be derived from basic physical properties. The quantity "unit stream power" ω, which is a measure of potential energy expended per unit bed area, can be calculated such that

$$\frac{dz}{dt} = k_b \omega^a \tag{1}$$

where a is a dimensionless exponent, z is the elevation of the river channel bed, and t is time. The rate coefficient k_b is expected to depend on sediment flux. A relationship for total stream power Ω, the potential energy expenditure for a unit length of channel, can be derived from a conservation of energy argument. Over a length of stream channel Δx with an elevation drop Δz and bedrock density ρ, the potential energy difference ΔPE over a volume of water V is

$$\Delta PE = \rho V g \Delta z . \tag{2}$$

To relate a change in potential energy back to total stream power Ω, ΔPE can be quantified as a unit change over a given time Δt and channel length Δx where

$$\frac{\Delta PE}{\Delta t \Delta x} = \Omega = \frac{\rho V g \Delta z}{\Delta t \Delta x}. \tag{3}$$

By defining water discharge as $Q = V/\Delta t$ and slope $S = \Delta z/\Delta x$, the above expression can be simplified to

$$\Omega = \rho g Q S. \tag{4}$$

Relating back to unit stream power ω gives

$$\omega = \frac{\Omega}{w} = \frac{\rho g Q S}{w}. \tag{5}$$

The relationship in Equation (5) can be more clearly understood by using the following two expressions for channel width w and discharge Q [Leopold and Maddock 1953; Dunne and Leopold 1978]

$$w = k_w Q^b \tag{6}$$

$$Q = k_q A^c = V/\Delta t \tag{7}$$

where the exponents are dimensionless. Using these relationships and returning to the unit stream power expression gives

$$\frac{dz}{dt} = E = k_b \omega^a = k_b \left(\frac{\rho g Q S}{w} \right)^a = k A^m S^n \tag{8}$$

where $n=a$, $m=ac(1-b)$, and E is erosion rate assuming no subsidence or uplift.

The exponents m and n vary depending on channel characteristics and the mechanisms driving channel incision with published ranges from $0.1 \leq m/n \leq 1$ [Seidl and Dietrich 1992; Stock and Montgomery 1999; Whipple and Tucker 1999]. Understanding the components of k is

integral to an analysis of the stream power law. Based on expressions for w and Q in Equations (6) and (7), the value of k can be decomposed such that

$$k = \frac{k_b k_q^{a(1-b)}}{k_w^a} \rho^a g^a \tag{9}$$

where k is a function of material strength k_b, hydrology k_q, hydraulic geometry k_w, rock density ρ, gravitational acceleration g, and dimensionless constants a and b. When this basic stream power model is applied to large-scale landscapes, significant correlation between erosional efficiency k and precipitation rates have not been observed in previous work [Riebe et al. 2001]. This study seeks a possible relationship between k and precipitation by explicitly incorporating precipitation into the stream power law, and applying the new formulation to bedrock river channels spanning a large precipitation gradient.

1.2 Stream Power and Precipitation

In this paper I will investigate the hypothesis that erosion rate is dependent on precipitation rate. To understand this relationship, I will reformulate the stream power law to contain a precipitation term by starting with the relationship that water discharge Q is related to mean annual precipitation $\overline{P}$ such that

$$Q = \gamma \overline{P} A^c \tag{10}$$

where c is constant and $\gamma \leq 1$ is a coefficient representing the percent of precipitation lost to evapotranspiration and infiltration. The true relationship with runoff, evapotranspiration, and infiltration may be more complicated (for example, high precipitation would likely effect plant growth, thus stimulating root growth and limiting infiltration but increasing evapotranspiration), but I propose Equation (10) as a reasonable approximation. The value of $\overline{P}$ can then be

approximated as runoff in the basin. Substituting Equation (10) into the expression for erosion in Equation (8) gives

$$E = k_b \left(\frac{\rho g \gamma \overline{P} A^c S}{w} \right)^a . \tag{11}$$

Recalling the expression for w is dependent on Q as shown in Equation (6), the expression in Equation (11) can be used to rewrite the stream power as

$$E = \varepsilon \overline{P}^{a(1-b)} A^{ac(1-b)} S^a \tag{12}$$

where ε is a constant. Finally, this equation can be rewritten for clarity with new variables as the multiple exponent expression

$$E = c_0 P^{C_P} A^{C_A} S^{C_S} \tag{13}$$

where c_0 is an efficiency coefficient and all quantities are measured. The form of the new multiple exponent relationship is very similar to that of the original stream power law, but it allows for a study of precipitation independently of other variables that contribute to erosional efficiency.

2 Methods

A controlled test of the precipitation-dependent stream power expression requires a landscape with measurable long-term erosion rates, a gradient in precipitation, and little variation in lithology and channel geometry. Volcanic islands are an excellent location to test this theory because they frequently are composed of relatively uniform lithology. Furthermore, precipitation gradients are often large due to orographic precipitation on mountains. For this analysis, I specifically look to the island of Kauai in the Hawaiian island chain. The island is composed of basalt flows, which likely exhibit minimal variability in bedrock erodibility. The basins studied

are on the western side of the island. These basins are almost entirely composed of Waimea Canyon basalts, which were assumed to have a constant density. Conducting a similar study in a location with non-constant lithology would introduce more variability since fluvial erosion rate varies with the square of tensile strength, and would likely obscure trends between erosion rates and precipitation rates [Sklar and Dietrich 2001]. The other key factor making Kauai an ideal study location is a steep rainfall gradient between the center of the island and the coast.

This thesis will focus on developing and quantifying the relationship between precipitation and erosion on Kauai. First an overview of the setting was conducted by researching the geology, topography, and climate of Kauai. Once the setting was established as a viable location for the study, a method of estimating erosion rates was developed. This method uses spline-fitting to predict the topography of the island at the end of its shield-building phase. These topography estimates were then used in conjunction with published geochronology data to calculate erosion rates around the island. Finally, data from the spline surfaces and the current topography were used to calculate and compare bedrock erosional efficiencies across the island. The erosional efficiencies were compared with modeled mean annual precipitation rates and the quantities were compared to the precipitation-dependent power law relationship developed.

2.1 Geology and topography of Kauai

The Hawaiian Islands are a volcanic island chain in the Pacific Ocean formed by hotspot volcanism in the Pacific plate. Kauai is the second oldest island in the chain. This study focused on 31 clearly delineated watersheds on the western side of Kauai as identified in Figure 2. Small basins on the western coast of Kauai were studied in groups of 3-5 for practical purposes. Each

watershed contains a main stream with branching smaller streams that flow into the main channel.

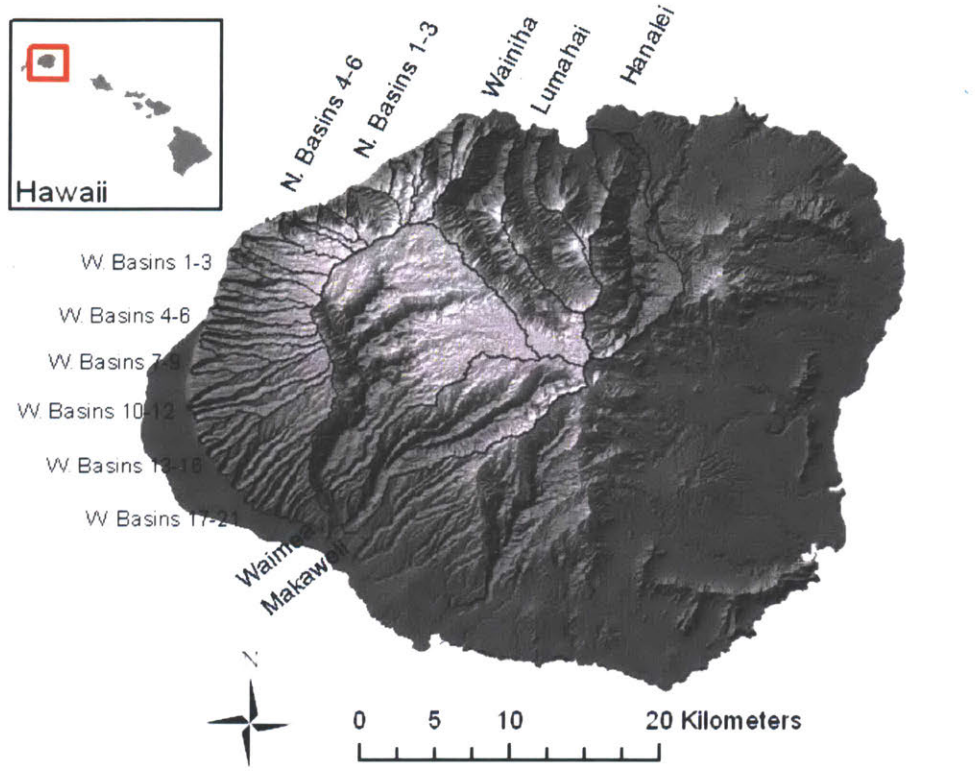

Figure 2: Map of Kauai. The watersheds studied are on the western side of the island. The small basins on the western coast were grouped together for practical purposes. The Hanalei basin was divided into eastern and western sides for the analysis.

The island of Kauai is composed of two major rock units: the Waimea Canyon Basalts and rejuvenated volcanism of the Koloa Volcanics [Macdonald et al. 1960]. The Waimea Canyon Basalts are further divided into three main formations, the Olokele, Napali, and Makaweli members (Figure 3). Kauai erupted in several main phases. The shield-building phase consisted of the eruption of the three main formations in the Waimea Canyon Basalts. The Napali member contains the oldest rocks of Kauai and composes the main shield of the volcano. Today the Napali member is primarily exposed on the western side of the island. After the formation of the Napali, the Olokele caldera collapsed in the center of the island and filled with thick basalt deposits. The final step of the main shield-building event occurred with the

formation of the Makaweli member graben on the southern side of the island. Rejuvenated Koloa volcanism erupted following the shield building phase, covering most of the eastern part of the island [Macdonald et al. 1960; McDougall 1979; Garcia et al. 2010].

Significant geochronology work has been conducted around Kauai to determine the age relationships between units (see appendix 7.1 for a summary of geochronology in Kauai). The Napali member has been dated between 3.43-5.77 Ma [Macdonald et al. 1960; McDougall 1979; Garcia et al. 2010], although McDougall [1979] noted that some of the samples in his study had experienced appreciable radiogenic argon loss, and suggested that the best estimate for the age of the Napali is 4.35±0.09 Ma. The Olokele member has been dated as 3.95-4.3 Ma [Macdonald et al. 1960; Clague and Dalrymple 1988] and the Makaweli member has been dated as 3.59-4.15 Ma [Macdonald et al. 1960; Clague and Dalrymple 1988; Garcia et al. 2010]. McDougall [1979] calculated an age for shield building of the island to be 4.43±0.45 Ma by weighting the results of numerous ages determined from the Napali and Makaweli members. Few samples have been dated from the Olokele formation due to poor accessibility for collecting samples. Garcia et al. [2010] dated the shield-building phase from 5.1-4.0 Ma with post-shield lavas erupting from 3.95-3.6 Ma. Rejuvenated volcanism began 1 Myr later, and lasted from 2.6-0.15 Ma.

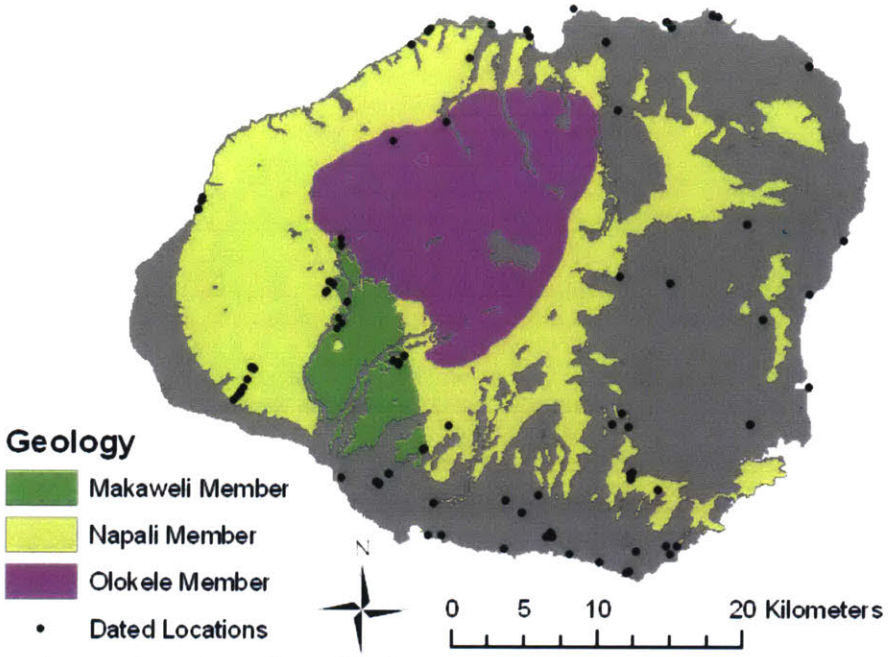

Figure 3: Kauai geology and geochronology. The three members of the Waimea Canyon Basalts – the Makaweli, Napali, and Olokele – are shown in color. Geochronology points from Clague and Dalrymple [1988], Everenden et al. [1964], Garcia et al. [2010], Hearty et al. [2005], McDougall [1964] and McDougall [1979]. Geologic map modified from Sherrod et al. [2007]. The ages associated with all points are given in Appendix 7.1.

2.2 Climate

Kauai is notable for its precipitation gradient across the island. In the central, wettest part of the island, the maximum mean annual precipitation rate is almost 9 m/year. On the dry coastal plains on the western side of the island, the minimum mean annual precipitation rate is about 0.49 m/yr [PRISM Climate Group]. Rainfall around Kauai is measured only at discrete weather stations, but for the purposes of this study, it was necessary to have a model of mean annual precipitation rates for the entire island. Traditionally, maps of such data have been constructed by hand by correlating point data with elevation and synoptic features. In recent years, a model has been developed to produce consistent, repeatable, high-quality digital climate maps at high resolutions. This model, known as PRISM (Parameter-elevation Regressions on Independent Slopes Model), is used in this study to estimate mean annual rainfall [Daly et al 2002].

PRISM uses an understanding of climate patterns to generate predictions that lead to the creation of high-resolution precipitation maps. Digital elevation models (DEMs) are the main basis for PRISM since climate varies very strongly with elevation. To calculate precipitation rates at a point on the map, data from each weather station are assigned weights based on their distance from the point of interest, elevation, clustering with respect to other stations, vertical layer, topographic facets, proximity to the coast, and effective terrain weights. PRISM uses a two-layer model to divide the atmosphere into a lower boundary layer and an upper free atmosphere layer to account for temperature inversions. These factors are accumulated and evaluated to construct a weighted climate-elevation regression method. The method assumes a linear regression between elevation and temperature and precipitation [Daly et al. 2002].

For this study, the Kauai mean annual precipitation data set was used and resampled to 10 m spacing to match the spacing of the DEM being used for the rest of this study. It was assumed that the precipitation gradient has been consistent across Kauai since the island formed. This assumption is justifiable since precipitation rates are most strongly dependent on overall elevation of the island, which has remained in a general shield shape with the highest elevations in the center of the island throughout Kauai's history. On Kauai, the center of the island is the wettest with mean annual precipitation decreasing radially outwards (Figure 4). The western coast of the island is the driest region. Some watersheds, including the Hanalei, Wainiha, Lumahai, and Waimea, span the large precipitation gradient between central Kauai and the coasts while smaller watersheds on the Napali coast in the west span relatively small precipitation gradients.

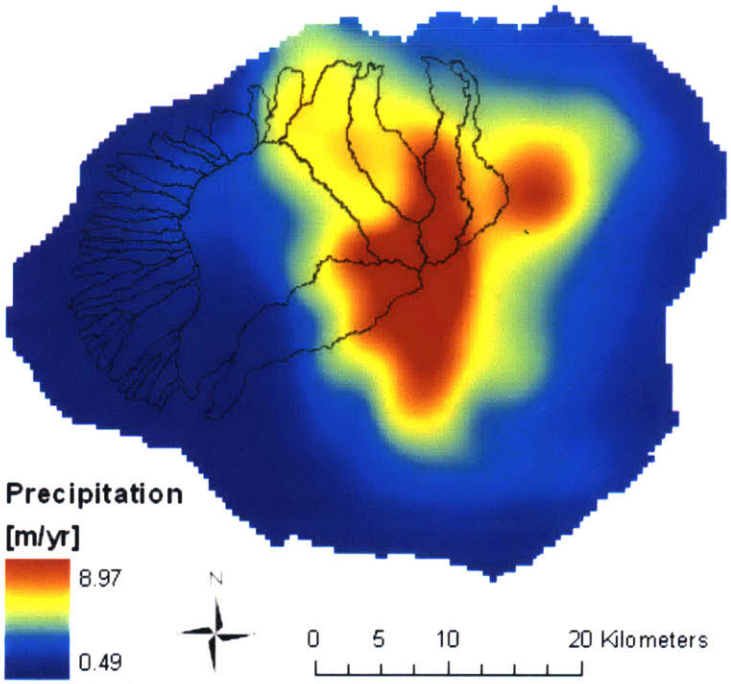

Figure 4: Mean annual precipitation as modeled by the PRISM climate model. Mean annual precipitation is highest in the center of the island and decreases radially outward.

2.3 Splines for estimating long-term erosion rates

To estimate the volume of rock eroded from Kauai since the island formed, I applied a quantitative method to approximate the original topography of the island. Existing methods for calculating erosion rates based on field data were inappropriate for million year timescales and existing data were too sparse. Many erosion rate studies use sediment yield as a proxy for erosion rate, but since sediment yield is only measured over annual or decadal time scales, the yields are likely to be highly influenced by anthropogenic disturbance and land use, which are not major factors over geologic time [Milliman et al. 1987]. More importantly, sediment flux measurements are only available in two of the basins studied, the Hanalei and Waimea basins. Cosmogenic nuclide data may also be used to calculate erosion rates, but these data are only applicable on a 1,000-10,000-year time scale. Similar to sediment flux data, cosmogenic nuclide

measurements are only taken at point locations, and in Kauai, measurements only exist for the Hanalei basin.

Since sediment flux and cosmogenic nuclide methods were insufficient, a new method to calculate long-term erosion rates was developed. The method uses currently present surfaces to create splines that are stretched over the current-day topography, similar to the approach taken by Brocklehurst and Whipple [2002]. The mean erosion rate since formation can be determined by subtracting the current day topography from the spline and dividing by the basin age. By examining hillshade relief maps of 10 m DEM data, it is possible to visually select surfaces that appear to have experienced little erosion since their eruption. These paleosurfaces are minimally dissected by streams and typically have higher elevations than their surroundings. The splines were anchored by the selected paleosurfaces and used a fitting method heavily weighted towards a least-squares fit. By creating splines over all basins of interest, a theoretical shape of the topography at the end of shield-building was developed. The spline method is outlined in Figure 5.

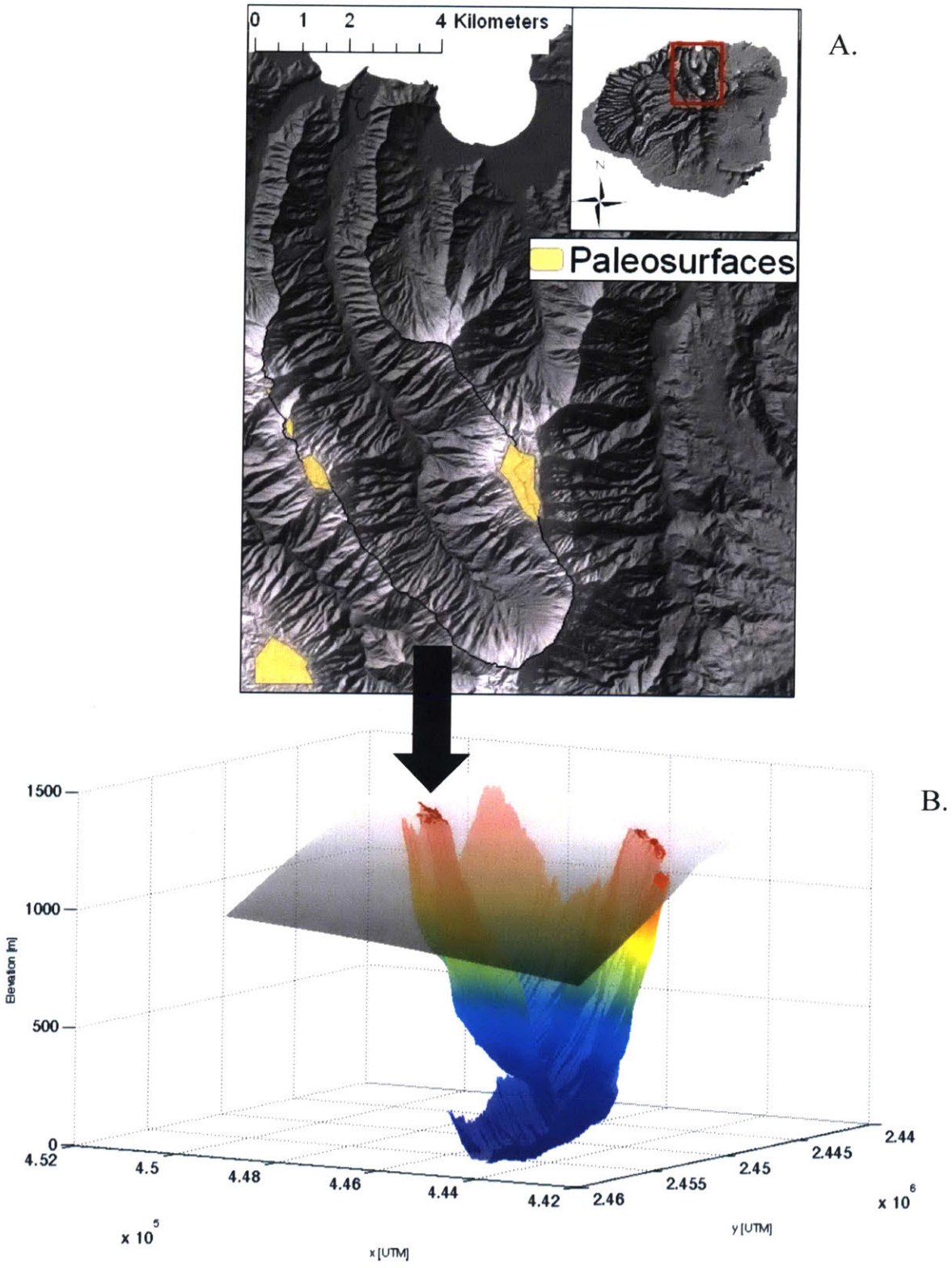

Figure 5: Example of spline fitting method for the Lumahai basin. A. Map view of the Lumahai basin. Uneroded paleosurfaces used as the basis for the spline are shown in yellow. B. Spline fit over the current topography. Current topography from 10 m DEM is in color, the spline fit surface is in gray. The process was replicated for each basin or group of basins

Each watershed with an area greater than 10 km^2 was studied individually while the smaller basins on the Napali coast were grouped in clusters of 3-5 basins for practical purposes. The Napali coast basins are comparable in geometry and topography, so grouping them together generated splines very similar to those that would have been created by studying each basin individually. The Hanalei basin was fit by separate splines on the western and eastern halves with the Hanalei River acting as the dividing line between the two sides. The eastern Hanalei is primarily composed of Koloa basalt flows with an age of about 1.46 Ma [Garcia et al. 2010] and has low topography while the western Hanalei runs through the Napali and Olokele members with an age of about 4.0 Ma [Macdonald et al. 1960] and has higher topography, so it was most logical to fit the sides separately.

Due to the segmented nature of the spline fitting, combining splines from each basin does not create a continuous shield for the island (Figure 6). Since the shield-building phase of the island lasted about 1.1 million years [Garcia et al. 2010], the initial shape was not likely a smooth shield. By fitting the basins separately instead of with one spline for the entire island, I account for the discrete time steps that occurred within the shield-building phase.

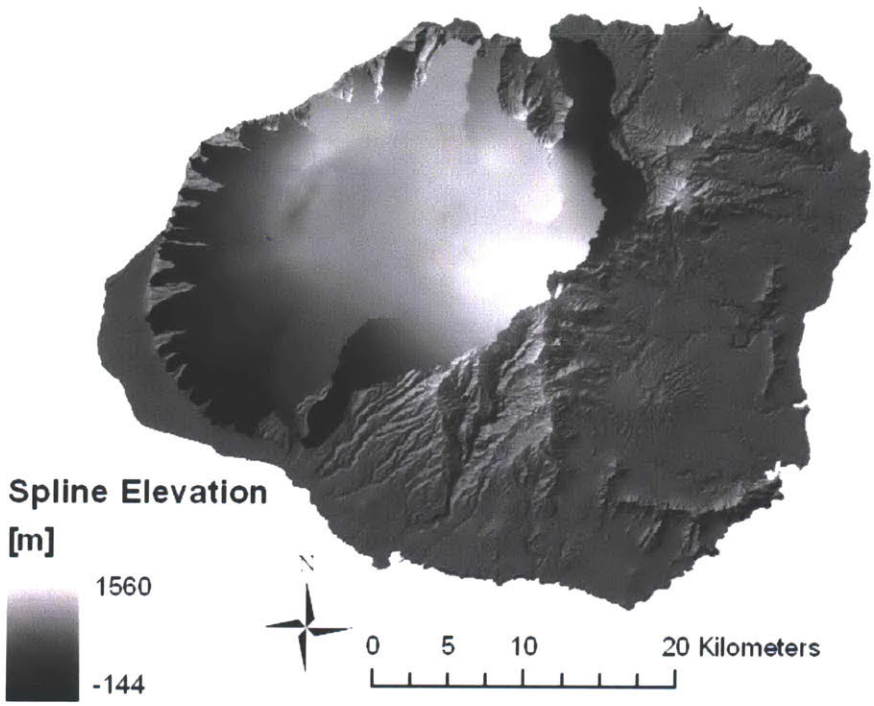

Figure 6: All spline surfaces for Kauai. Splines are not completely continuous because each spline was calculated independently of the others.

One weakness to the spline fitting method is that it relies on the presence of identifiable uneroded initial surfaces. In most of the basins, sufficient surfaces exist to use this method. In some regions, most notably in the area covered by the Makaweli formation, uneroded surfaces no longer appear to exist. In these cases, small ridges of highest topography that appeared to be minimally dissected by streams were used for creating the spline fit. In all cases, the spline fit is a minimum estimate for initial topography. In the case of the Makaweli formation splines, the fits are almost definitely lower than the paleotopography since few paleosurfaces still remain near the basin. The spline fitting method clearly introduces a large measure of uncertainty into calculations, but since no other method exists to better approximate paleotopography, this uncertainty was accepted as potential error in the method.

Another notable characteristic of the spline fits is that they do not meet the current coastlines near the outlet in most locations, most notably in the Lumahai, Wainiha, and Northern

Basins 1-3. When considering this discontinuity, it is important to note that the paleoshorelines of Kauai were not the same at the time of formation as they are today. Flinders et al. [2010] used gravity measurements to reconstruct the paleoshorelines around Kauai. For most of the island, the paleoshoreline extended 5-10 km past the current-day coasts. Subsidence, erosion, and mass-wasting events have since created the shape of the island seen today. The discontinuity between the splines and the current day coasts does not necessarily mean that the splines are inaccurate; their shape instead may be explained by changes in the island's overall topography since formation.

One major assumption made as part of this method was that watershed outlines have remained constant over time. Although rivers and watersheds may shift, the distinctive ridges in the topography of Kauai, in conjunction with the uneroded surfaces still present, imply that the watersheds have remained in relatively the same locations for much of the island's history.

Eroded volumes were calculated by subtracting the modern topography of the island from the theoretical elevation of the spline fits. The volumes were converted to rates by dividing the eroded volume by the age of the currently exposed rocks. Since geochronology has not been conducted in every basin of Kauai, some assumptions were necessary to assign ages to all basins. In general, each basin was assigned a single age based on the youngest exposed rock within the basin. The exception to this rule is that deposits of young Koloa volcanics were not considered when assigning ages to any of the basins except for the eastern Hanalei. In all of the basins except the eastern Hanalei, the Koloa volcanics make up only a minimal portion of the basin by volume and are very thin. Since the majority of the eastern Hanalei is composed of Koloa volcanics, these ages were considered. Table 1 shows the ages used to calculate erosion rates for

each basin. In the case of basins without any published ages, the ages of nearby basins of similar lithology were used.

Table 1: Basin Geochronology. Minimum ages for each basin were used to calculate erosion rates.

Basin	Age (Ma)	Source
Hanalei East	1.46	Garcia et al. 2010
Hanalei West	4.0	Macdonald et al. 1960
Lumahai	4.0	Macdonald et al. 1960
Wainiha	4.0	Macdonald et al. 1960
N. Basins 1-3	3.81	McDougall 1979
N. Basins 4-6	3.81	McDougall 1979
W. Basins 1-3	3.93	McDougall 1979
W. Basins 4-6	3.93	McDougall 1979
W. Basins 7-9	3.93	McDougall 1979
W. Basins 10-12	4.51	McDougall 1979
W. Basins 13-16	4.51	McDougall 1979
W. Basins 17-21	4.51	McDougall 1979
Waimea	3.6	McDougall 1964
Makaweli	3.91	Clague & Dalrymple 1988

2.4 Topographic analysis to measure drainage area and slope

In order to conduct a precipitation-dependent stream power analysis of the form derived in Equation (13), several physical features of the landscape need quantification. Slope S and drainage area A were calculated from 10 m DEM maps at each pixel in the map. Slopes were calculated from the present-day topography using the eight nearest neighbor pixels to determine a local slope at each pixel in the map. Slopes of the spline surfaces were not used in the equation because local slopes varied highly with details of the spline fit. The spline fits create a good overall model for erosion over a basin, but the slopes at individual locations may be misleading due to the boundary conditions of the splines. Although slopes of the current river profiles are not the same as the slopes of paleorivers, they are the best approximation that can be made with this method.

Upstream drainage area at each point was calculated using the flow accumulation tool in ArcGIS. To differentiate fluvially dominated bedrock channels from the surrounding topography, a drainage area cutoff of greater than 10^5 m^2 was used [Montgomery and Foufoula-Georgiou 1993]. To test the applicability of this cutoff to Kauai, the stream networks with drainage area greater than 10^5 m^2 were visually examined and compared with hillshade maps and aerial imagery from Google Earth. This check confirmed that the selected channels appeared to be in bedrock reaches. Based on these findings, only locations that have a drainage area greater than 10^5 m^2 were included in stream power calculations.

3 Results

Erosion rates were calculated across the basins by subtracting the current topography from the spline fit and dividing by the mean basin age as given in Table 1. Mean erosion rates for each basin are given in Table 2.

Table 2: Mean erosion rates for each basin. Volume eroded is based on the spline fit and assumes a constant rock density of 3000 kg/m^3.

Basin	Area [km^2]	Volume Eroded [km^3]	Erosion rate [mm/yr]	Erosion rate [t/km^2/yr]
Hanalei East	22.72	1.82	0.05	164.89
Hanalei West	37.29	18.09	0.12	363.84
Hanalei Total*	60.01	19.91	0.10	288.52
Lumahai	35.83	24.13	0.17	505.15
Makaweli	68.70	16.37	0.06	182.83
N. Basins 1-3	24.96	9.04	0.10	285.23
N. Basins 4-6	12.41	2.18	0.05	138.32
W. Basins 1-3	23.28	1.54	0.02	50.50
W. Basins 4-6	15.79	0.81	0.01	38.95
W. Basins 7-9	16.45	0.81	0.01	37.37
W. Basins 10-12	24.66	1.11	0.01	30.00
W. Basins 13-16	28.88	1.50	0.01	34.57
W. Basins 17-21	15.86	0.41	0.01	17.12
Waimea	146.36	33.98	0.06	193.47
Wainiha	58.29	31.81	0.14	409.29

*Hanalei total values are an area-weighted average of the Eastern and Western Hanalei Basins

A plot of erosion rates against basin-averaged mean annual precipitation is shown below in Figure 7. The same data are shown in Figure 8 averaged for each basin group. The values on the x-axis, basin-averaged mean annual precipitation, were calculated by summing upstream precipitation and dividing by drainage area. Due to the density of data points from DEMs, plots show the individual data points in small black dots and the same data divided into fifty bins in the larger colored circles. Trends are much more clearly visible in the binned data. Outliers where precipitation rates were less than 0.6 m/yr or more than 10 m/yr were considered to be errors in the PRISM model and are not shown in the plots.

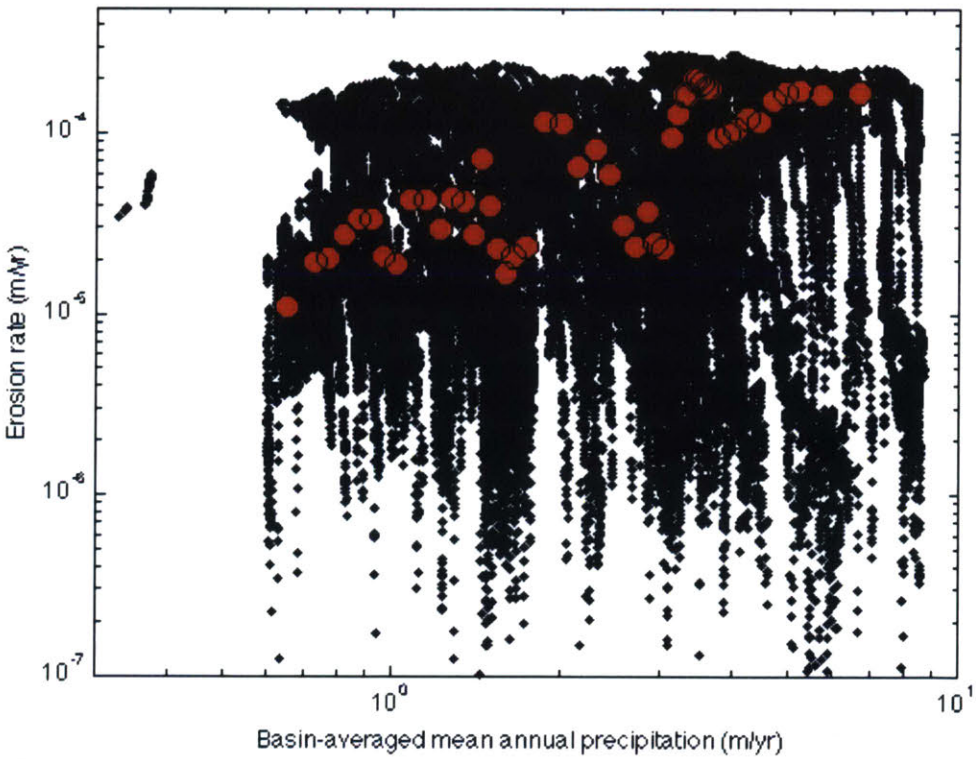

Figure 7: Erosion rate vs. basin-averaged mean annual precipitation. Data shown are for all basins in the study. Erosion rate increases exponentially with mean annual precipitation. For binned data shown r^2=0.627.

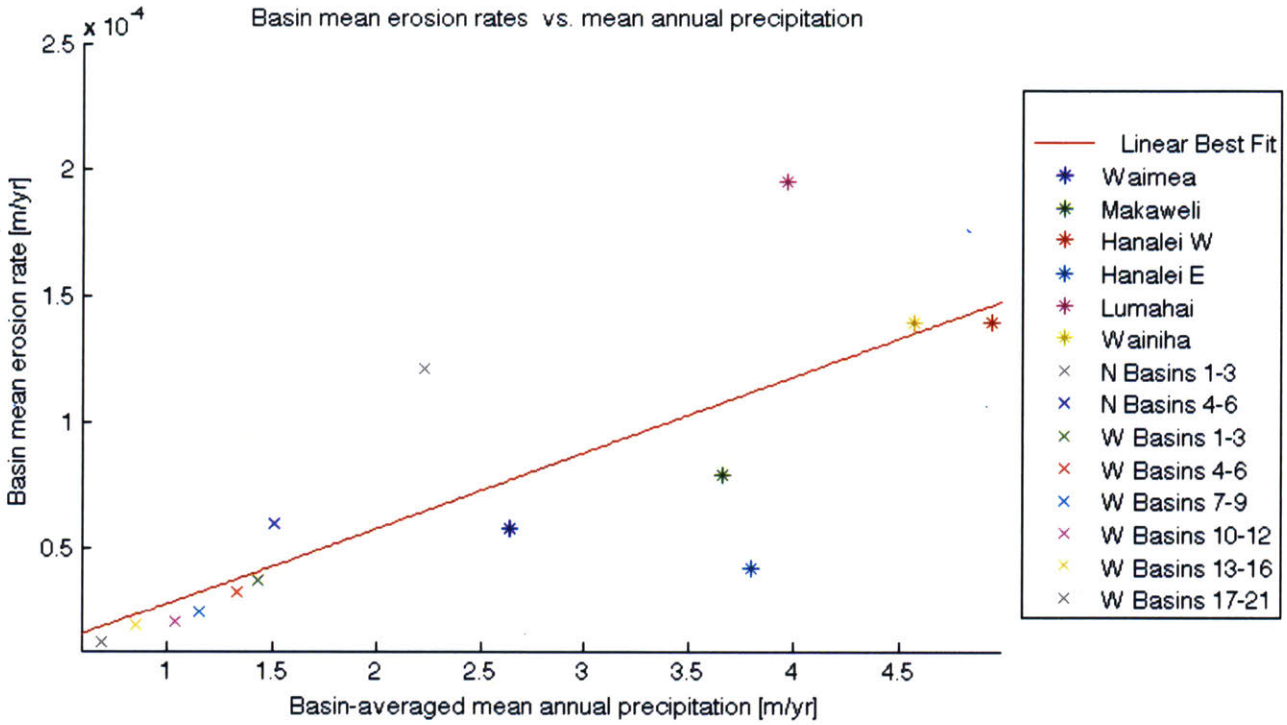

Figure 8: Basin-averaged erosion rate vs. basin-averaged mean annual precipitation for each basin. Note the linear scale on both axes. A linear fit is best for this data set and gives r^2=0.62. As with the entire dataset in Figure 7, erosion rate increases with basin-averaged mean annual precipitation.

Although a trend appears to exist in the plot of erosion rate versus basin-averaged mean annual precipitation, the trend is still somewhat weak. To test the dependence of erosional efficiency on precipitation, a multiple regression analysis of the form shown in Equation (12) was conducted. The precipitation-dependent stream power analysis resulted in the trend shown in Figure 9 between erosional efficiency and basin-averaged mean annual precipitation.

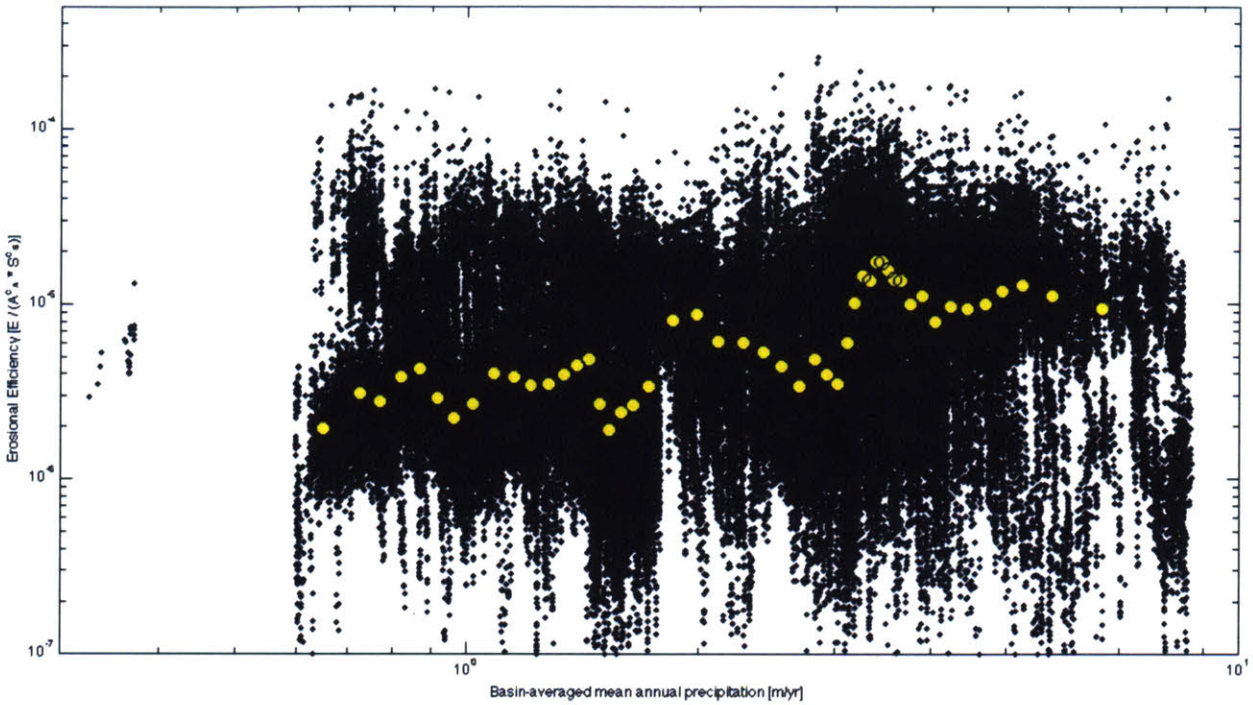

Figure 9: Precipitation-dependant erosional efficiency vs. basin-averaged mean annual precipitation. Data shown is for all basins in the study. A trend exists positively correlating erosional efficiency with basin-averaged mean annual precipitation. For all data, r^2=0.25, for binned data shown r^2=0.629.

By modeling erosion with the precipitation-dependent formulation of the stream power law, a trend arises. Erosional efficiency is positively correlated with basin-averaged mean annual precipitation. The values of the exponents in the law were calculated using a multiple regression analysis. The relationships between the exponents in the proposed power law and the constants used in previous expressions are given below in

Table 3, along with experimentally determined values for each exponent for Kauai.

Table 3: Precipitation-dependent stream power exponents.

	Equivalent stream power expression	Experimental values
C_P	m/c	0.44
C_A	m	0.24
C_S	n	0.65

4 Analysis and Discussion

4.1 Erosion, erosional efficiency, and precipitation rates

The multiple regression stream power analysis (Figure 9) indicates a clear link between precipitation and erosional efficiency. In contrast to the findings of Riebe et al. [2001], a comparison of erosion rate versus precipitation shows correlation between the data (Figure 7). Erosion rates increase with basin-averaged mean annual precipitation, as predicted by basic analysis of the stream power law. In their analysis of erosion rates, Riebe et al. [2001] measured erosion rates with cosmogenic nuclides at seven sites, assigning a single erosion rate and a single average precipitation rate to each site and then comparing the seven data points to find no correlation. The approach of this study, to examine erosion rates across a precipitation gradient at a single location, allows for more direct comparisons and gives a dataset of over 100,000 points. This method minimizes the effect of the possibility of lithologic differences across sites, since Kauai has constant lithology.

Although there is a definite correlation that arises from the multiple regression analysis, the trend has high variability as noted by the low r^2 value. Due to this variability, a signal may not have arisen in previous studies with only a low volume of data. The availability of 10 m DEMs and computing software gives a dataset of over 100,000 points located in a bedrock channel as defined by a drainage cutoff of 10^5 m^2. Previous studies have relied on data manually calculated from topographic maps and field studies, methods which limit the potential number of data points to the data that can be practically produced. With so few data points and high natural variability, the trend might not have been apparent in previous work.

Furthermore, Kauai's precipitation gradient is substantially higher than the gradients observed at field sites that have been used in other studies. Whereas the studies summarized by

Riebe et al. [2001] extend to a maximum precipitation rate of only about 2 m/yr, mean annual precipitation rates on Kauai range from less than 0.5 m/yr to over 8.5 m/yr. Because of the high variability in the data, a study conducted over a smaller precipitation gradient would probably have produced data with a less significant trend. In short, although the trend in Kauai can be applied to other locations, the conclusions drawn from this analysis may not have immediately appeared in studies at other field sites.

Although it is interesting for comparison purposes to examine the trend between precipitation rates and erosion rates, it is more significant to study the trend between the erosional efficiency coefficient and precipitation rates. Erosional efficiency indicates not just the volume of material eroded over time, but also provides insight into the mechanics of long-term erosional processes. The correlation between erosion rates and precipitation rates is expected not only because of a physical understanding of erosional processes, but also because of the radial symmetry of Kauai with respect to slope and drainage area distribution around the sampled basins. By determining that erosional efficiency is also positively correlated with precipitation rates, I am able to show that the trend is not simply a result of the island's symmetry.

The next step of this work is to understand if this relationship holds true for other bedrock channels of uniform lithology. In theory, the relationship should apply to other ocean islands and to continental landscapes, although this theory has not yet been tested. Further application of the precipitation-dependent formulation of the stream power law in Equation (13) will help quantify and test its applicability to a range of field sites.

4.2 Exponent Values

Relating the experimentally determined values of m=0.24 and n=0.65 back to the initial stream power law provides a point of comparison between this project and previous publications. Published values of the ratio m/n range from 0.1 to 1.0. My calculated ratio m/n=0.37 falls within this range. For a region like Kauai, where the paleoprofile of many basins are relatively flat, the value of n is difficult to constrain and is frequently taken to be 1 [Seidl and Dietrich 1992; Stock and Montgomery 1999; Whipple and Tucker 1999]. Initially, Seidl and Dietrich [1992] calculated m=n=1 in costal Oregon, and Seidl et al. [1994] later applied these values to channels on western Kauai to model stream profile development in bedrock. Stock and Montgomery [1999] found that m varied between 0.1 and 0.2 if n was allowed to vary widely. Whipple and Tucker [1999] more narrowly constrained m/n to range between 0.35 – 0.6. My calculated ratio falls within this range.

By modeling erosion as a power law with exponents on each term, I investigate the dependence of erosion on precipitation, drainage area, and slope. Based on the experimentally determined values of the exponents in

Table 3, erosion is most dependent on slope, has an intermediate dependence on precipitation, and has the lowest dependence on drainage area. The precipitation-dependent stream power law can now be rewritten with the exponent values as

$$E = c_0 P^{0.44} A^{0.24} S^{0.65} \tag{14}$$

where c_0 is a coefficient that varies with bed material and channel geometry.

4.3 Shear stress and stream power models

Throughout this study, the stream power law has been used to model bedrock river incision. Alternatively, I now consider the applicability of the results to a shear stress model based on conservation of momentum and conservation of mass of water ($Q = wh\bar{u}$) as proposed by Howard and Kerby [1983]. The shear stress model takes a very similar form to the stream power model, but results in different exponent and coefficient values. Comparing the experimentally determined exponents to the expected exponents for stream power and shear stress may indicate which law more closely models river incision in Kauai. The brief explanation below indicates the origin of the shear stress model, following the derivation of Snyder et al. [2000].

Based on conservation of momentum, shear stress τ_b is defined as

$$\tau_b = \rho g h S = \rho C_f \bar{u}^2 \tag{15}$$

Rearranging the above equation and substituting in the conservation of mass for water equation gives a general form of

$$\tau_b = k_t (Q/w)^{\alpha} S^{\beta} \tag{16}$$

where α and β are dimensionless. Recalling Equation (6), the above expression can be further generalized as

$$\tau_b = \frac{k_t}{k_w^{\alpha}} Q^{\alpha(1-b)} S^{\beta}. \tag{17}$$

Using the expression for Q given in Equation (7), the shear stress equation can be rewritten as

$$\tau_b = \frac{k_t k_q^{\alpha(1-b)}}{k_w^{\alpha}} A^{\alpha c(1-b)} S^{\beta}. \tag{18}$$

The main difference between this shear stress erosion model and the stream power erosion model used in the experimental section of this project is the theorized values of the exponents. Based on Howard and Kerby's [1983] assumption that incision rates are linearly proportional to bed shear

stress, the expected value of the exponent on A is $m=\alpha c(1-b)=1/3$ and the exponent on S is $n=\beta=2/3$. The experimentally determined exponent values given in Table 3 on area and slope are 0.24 and 0.65, respectively. These values, especially the slope exponent, are extremely close to the expected values for the shear stress model. This finding indicates that the shear stress model may be a better fit to the physical processes of bedrock river incision on Kauai than the stream power model.

4.4 Error and statistical significance

A test of the statistical significance of the trend between erosional efficiency of precipitation-dependent stream power and basin-averaged mean annual precipitation gives $r^2=0.25$. This r^2 value is very low, but it is explained by the naturally high variance in the data. For the binned data shown, $r^2=0.62$. Erosion rates and drainage areas varied highly within each basin and between basins. The measurements of slope introduced the most noise into the data since slope can vary dramatically on local scales. Neighboring pixels in a DEM may have steeply differing slopes due to local details in the landscape or errors in the DEM. Future studies could decrease the error introduced by slope by sampling slopes over a longer reach of longitudinal distance or elevation. This method would smooth slopes and minimize the effects of waterfalls and knickpoints, to which stream power does not apply [Seidl et al. 1994].

4.5 Long- and Short-term Erosion Rates

Although this study used spline surfaces as the basis for calculating erosion rates, other commonly used methods to calculate erosion rates include measuring sediment flux at a stream gauge station or using cosmogenic nuclides. In this section, I will compare the erosion rates from

the spline fit method to the erosion rates calculated for the same regions using other methods. Spline fit erosion rates were converted from m/year to tons/km^2/yr by assuming a constant rock density of 3000 kg/m^3.

Sediment flux data from USGS stream gauge stations are available for two basins, the Hanalei and the Waimea. To compare the rates from the spline fit to the sediment flux rates in the Hanalei basin, the spline erosion rates from the eastern and western Hanalei were weighted by area and added. Daily sediment flux data from the Hanalei from 10/1/2003 – 9/30/2009 were used although there is a gap in the data from October 2006-October 2007. The mean sediment flux erosion rate calculated for these 6 years in the Hanalei basin is 368 tons/km^2/yr, assuming that the USGS data is reported in US tons. The mean long-term erosion rate from the spline for the entire Hanalei basin is 288.5 tons/km^2/yr. Sediment data from the Waimea was not as consistently or regularly sampled. Records began in January 1975 and are present through December 1994, but each year has only a mean of 8 samples. The mean erosion rate from the sediment flux in the Waimea during this period is 395 tons/km^2/yr while the mean long-term rate from the spline is 193 tons/km^2/yr.

As expected, long-term erosion rates from the splines are lower than rates calculated from data spanning a few years. As mentioned earlier, the spline fits represent a minimum elevation since they are tied down to current topography. In some locations, the paleosurfaces of the island are likely to have actually been higher than estimated by the splines. Nonetheless, since the erosion rates from the splines are on the same order of magnitude as the stream gauge erosion rates, they imply that long-term erosion rates are similar to those observed today.

Cosmogenic nuclide measurements provide another method for calculating erosion rates on a 1,000-10,000-year time scale. The long-term erosion rate estimated for the Hanalei basin by

cosmogenic nuclides is 286 tons/km^2/yr [K. Ferrier unpublished data, 2011], which is almost exactly the same as the value estimated by the splines of 288.5 tons/km^2/yr. Cosmogenic nuclide data is not available for the rest of the island. Further comparisons between spline rates and cosmogenic nuclide rates would strengthen the apparent agreement of the two methods. Overall, there is general agreement among erosion rates calculated from the spline fits, sediment gauges, and cosmogenic nuclides.

5 Conclusions

By studying the major basins on the western side of Kauai, splines can be used to reconstruct a theoretical initial surface for the island. In conjunction with geochronologic measurements, these splines can be used to determine long-term erosion rates since the formation of Kauai. Using these erosion rates, I have observed correlation between precipitation rates and erosion rates and precipitation rates and erosional efficiency. These observations substantiate the incorporation of a precipitation term into the stream power law.

The stream power law is used in a wide variety of modeling studies yet the exponents and the coefficient of erosional efficiency are still not well defined by previous literature [Snyder et al. 2000]. Using the multiple-regression analysis to further constrain the components of stream power is useful in increasing the accuracy of studies that rely on stream power to quantify bedrock channel incision. The new derivation of the stream power law could also be used in studies of continental bedrock channels where lithology is constant across the study reach.

Overall, this project indicates that contrary to the findings of Riebe et al. [2001], there is a power law relationship between precipitation rates and erosion and also between precipitation rates and erosional efficiency on Kauai. This relationship may not have been noticed in previous

studies because natural data variability is high, but using 10 m DEMs and a field site with a very high precipitation gradient allows a trend to show through the variability. Now that the trend has been quantified, it can be tested in other field areas to further advance and clarify the model. If this precipitation-dependent stream power relationship is universally true, it provides useful insight to long-term bedrock channel geomorphology and stream power models.

6 References

Brocklehurst, S. H., and K. X. Whipple (2002), Glacial erosion and relief production in the Eastern Sierra Nevada, California, *Geomorphology, 42*, 1-24.

Clague, D. A., and G. B. Dalrymple (1988), Age and petrology of alkalic postshield and rejuvenated-stage lava from Kauai, Hawaii, *Contributions to Mineralogy and Petrology, 99*, 202-218.

Daly, C., W. P. Gibson, G. H. Taylor, G. L. Johnson, and P. Pasteris (2002), A knowledge-based approach to the statistical mapping of climate, *Climate Research, 22*, 99-113.

Dunne, T., L. D. Leopold (1978), *Water in Environmental Planning*, W. H. Freeman and Company, New York.

Evernden, J. F., D. E. Savage, G. H. Curtis, and G. T. James (1964), Potassium-argon dates and the Cenozoic mammalian chronology of North America, *American Journal of Science, 262*, 145-198.

Flinders, A. F., G. Ito, and M. O. Garcia (2010), Gravity anomalies of the Northern Hawaiian Islands: Implications on the shield evolutions of Kauai and Niihau, *Journal of Geophysical Research, 115*.

Garcia, M. O., L. Swinnard, D. Weis, A. R. Greene, T. Tagami, H. Sano, and C. Gandy (2010), Petrology, geochemistry and geochronology of the Kaua'i Lavas over 4.5 Myr: Implications for the origin of rejuvenated volcanism and the evolution of the Hawaiian plume, *Journal of Petrology, 51*(7), 1507-1540.

Hearty, P. J., D. B. Karner, P. R. Renne, S. L. Olson, and S. Fletcher (2005), $^{40}Ar/^{39}Ar$ age of a young rejuvenation basalt flow: implications for the duration of volcanism and the timing

of carbonate platform development during the Quaternary on Kaua'i, Hawaiian Islands, *New Zealand Journal of Geology and Geophysics, 48*, 199-211.

Howard, A. D., and G. Kerby (1983), Channel changes in badlands, *Geological Society of America Bulletin, 94*, 739-752.

Leopold, L. D., T. J. Maddock (1953), The hydraulic geometry of stream channels and some physiographic implications, *Geological Survey Professional Paper, 253*.

Macdonald, D. A., D. A. Davis, and D. C. Cox (1960), Geology and groundwater resources of the island of Kauai, Hawaii, *Hawai'i Division of Hydrography Bulletin, 13*.

McDougall, I. (1964), Potassium-argon ages from lavas of the Hawaiian Islands, *Bulletin of the Geological Society of America, 75*, 107-128.

McDougall, I. (1979), Age of shield-building volcanism of Kauai and linear migration of volcanism of in Hawaiian island chain, *Earth and Planetary Science Letters, 46*, 31-42.

Milliman, J. D., Y. -. Qin, M. -. Ren, and Y. Saito (1987), Man's influence on the erosion and transport of sediment by Asian rivers: The Yellow River (Huanghe) example, *Journal of Geology, 95*, 751-762.

Montgomery, D. R., and E. Foufoula-Georgiou (1993), Channel network source representation using digital elevation models, *Water Resources Research, 29*(12), 3925-3934.

Portenga, E. W., and P. R. Bierman (2011), Understanding Earth's eroding surface with ^{10}Be, *GSA Today, 21*(8).

PRISM Climate Group, Oregon State University. http://prism.oregonstate.edu, accessed 15 September 2011.

Riebe, C. S., J. W. Kirchner, D. E. Granger, and R. C. Finkel (2001), Minimal climatic control on erosion rates in the Sierra Nevada, California, *Geology, 29*(5), 447-450.

Seidl, M. A., and W. E. Dietrich (1992), The problem of channel erosion into bedrock, *Catena Supplement, 23*, 101-124.

Seidl, M. A., W. E. Dietrich, and J. W. Kirchner (1994), Longitudinal profile development into bedrock: An analysis of Hawaiian channels, *The Journal of Geology, 102*, 457-474.

Seidl, M. A., R. C. Finkel, M. W. Caffee, G. B. Hudson, and W. E. Dietrich (1996), Cosmogenic isotope analyses applied to river longitudinal profile evolutions: Problems and interpretations, *Earth Surface Processes and Landforms, 22*, 195-209.

Sherrod, D. R., J. M. Sinton, S. E. Watkins, and K. M. Brunt (2007), Geologic map of the State of Hawai`i: U.S. Geological Survey Open-File Report 2007-1089.

Sklar, L. S., and W. E. Dietrich (2001), Sediment and rock strength controls on river incision into bedrock, *Geology, 29*(12), 1087-1090.

Snyder, N. P., K. X. Whipple, G. E. Tucker, and D. J. Merritts (2000), Landscape response to tectonic forcing: Digital elevation model analysis of stream profiles in the Mendocino triple junction region, northern California, *Geological Society of America Bulletin, 112*, 1250-1263.

Stock, J. D., and D. R. Montgomery (1999), Geologic constraints on bedrock river incision using the stream power law, *Journal of Geophysical Research, 104*(B3), 4983-4993.

USGS. USGS Water Data for USA. http://waterdata.usgs.gov/nwis, accessed 15 September 2011.

Whipple, K. X. (2004), Bedrock rivers and the geomorphology of active orogens, *Annual Review of Earth and Planetary Sciences, 32*, 151-185.

Whipple, K. X., and G. E. Tucker (1999), Dynamics of the stream-power river incision model: Implications for height limits of mountain ranges, landscape response timescales, and research needs, *Journal of Geophysical Research, 104*(B8), 17661-17674.

7 Appendix: Geochronologic Measurements of Kauai Volcanic Flows

Sample Number	Age [Ma]	1 sig. error	Longitude [WGS84]	Latitude [WGS84]	Stratigraphic Unit	Reference
75K3	0.52	0.02	-159.332	22.052	Koloa Volcanics	Clague and Dalrymple 1988
76K1	0.55	0.02	-159.363	22.035	Koloa Volcanics	Clague and Dalrymple 1988
75K1	0.65	0.03	-159.522	21.913	Koloa Volcanics	Clague and Dalrymple 1988
75K16	0.97	0.05	-159.502	21.897	Koloa Volcanics	Clague and Dalrymple 1988
75K2	1.09	0.04	-159.332	21.993	Koloa Volcanics	Clague and Dalrymple 1988
74K14	1.15	0.02	-159.490	21.886	Koloa Volcanics	Clague and Dalrymple 1988
65Ka1	1.22	0.07	-159.425	22.220	Koloa Volcanics	Clague and Dalrymple 1988
75K15	1.22	0.06	-159.502	21.897	Koloa Volcanics	Clague and Dalrymple 1988
74K13	1.25	0.03	-159.502	21.897	Koloa Volcanics	Clague and Dalrymple 1988
75K14	1.25	0.07	-159.502	21.897	Koloa Volcanics	Clague and Dalrymple 1988
74K3	1.26	0.08	-159.585	21.898	Koloa Volcanics	Clague and Dalrymple 1988
75K4	1.27	0.06	-159.310	22.085	Koloa Volcanics	Clague and Dalrymple 1988
65Ka2	1.28	0.03	-159.425	22.220	Koloa Volcanics	Clague and Dalrymple 1988
74K12	1.33	0.07	-159.502	21.897	Koloa Volcanics	Clague and Dalrymple 1988
74K2	1.44	0.04	-159.511	21.924	Koloa Volcanics	Clague and Dalrymple 1988
76K9	1.71	0.09	-159.582	21.919	Koloa Volcanics	Clague and Dalrymple 1988
74K6	1.83	0.04	-159.643	21.934	Koloa Volcanics	Clague and Dalrymple 1988
86KA2	1.91	0.02	-159.602	22.012	Koloa Volcanics	Clague and Dalrymple 1988
76K6	2.01	0.04	-159.519	22.213	Koloa Volcanics	Clague and Dalrymple 1988
74Wa9	2.59	0.06	-159.575	22.159	Koloa Volcanics	Clague and Dalrymple 1988
86KA12	3.65	0.03	-159.650	22.057	Koloa Volcanics	Clague and Dalrymple 1988
KA1237	0.62	--	-159.506	21.897	Koloa Volcanics	Evernden et al. 1964
KA1211	1.21	--	-159.503	21.900	Koloa Volcanics	Evernden et al. 1964
KV03-11	0.15	0.02	-159.471	21.882	Koloa Volcanics	Garcia et al. 2010
KV03-12	0.219	0.016	-159.452	21.875	Koloa Volcanics	Garcia et al. 2010
KV05-2	0.22	0.03	-159.431	21.928	Koloa Volcanics	Garcia et al. 2010
KV03-6	0.227	0.005	-159.450	21.876	Koloa Volcanics	Garcia et al. 2010
KV05-3	0.23	0.02	-159.431	21.928	Koloa Volcanics	Garcia et al. 2010
KV03-8	0.32	0.018	-159.419	21.892	Koloa Volcanics	Garcia et al. 2010
KV03-10	0.32	0.09	-159.446	21.888	Koloa Volcanics	Garcia et al. 2010
KV03-7	0.324	0.007	-159.426	21.892	Koloa Volcanics	Garcia et al. 2010
KV05-14	0.419	0.014	-159.425	22.058	Koloa Volcanics	Garcia et al. 2010
KV03-27	0.52	0.05	-159.534	21.890	Koloa Volcanics	Garcia et al. 2010
KV05-1	0.68	0.02	-159.576	21.899	Koloa Volcanics	Garcia et al. 2010
KR-3	0.69	0.03	-159.398	22.227	Koloa Volcanics	Garcia et al. 2010
KV03-15	0.94	0.03	-159.463	21.969	Koloa Volcanics	Garcia et al. 2010
KV03-20	1.22	0.02	-159.456	21.976	Koloa Volcanics	Garcia et al. 2010
KV04-1	1.22	0.07	-159.333	22.195	Koloa Volcanics	Garcia et al. 2010
KV04-13	1.22	0.03	-159.333	22.195	Koloa Volcanics	Garcia et al. 2010
KV04-9	1.29	0.03	-159.428	22.223	Koloa Volcanics	Garcia et al. 2010
KV03-21	1.35	0.02	-159.533	21.920	Koloa Volcanics	Garcia et al. 2010
KV04-8	1.44	0.03	-159.429	22.223	Koloa Volcanics	Garcia et al. 2010
KV03-18	1.46	0.03	-159.371	21.969	Koloa Volcanics	Garcia et al. 2010
KV04-3	1.46	0.03	-159.469	22.210	Koloa Volcanics	Garcia et al. 2010
KV03-19	1.47	0.03	-159.452	21.967	Koloa Volcanics	Garcia et al. 2010
KV04-4	1.49	0.02	-159.469	22.210	Koloa Volcanics	Garcia et al. 2010
KV03-17	1.55	0.03	-159.371	21.969	Koloa Volcanics	Garcia et al. 2010
KV05-15	1.57	0.05	-159.374	22.095	Koloa Volcanics	Garcia et al. 2010
KR-2	1.67	0.08	-159.394	22.227	Koloa Volcanics	Garcia et al. 2010
0301-4	1.75	0.03	-159.571	21.968	Koloa Volcanics	Garcia et al. 2010
KV03-1	1.81	0.07	-159.611	21.937	Koloa Volcanics	Garcia et al. 2010
KV03-3	1.83	0.04	-159.618	21.931	Koloa Volcanics	Garcia et al. 2010

Sample Number	Age [Ma]	1 sig. error	Longitude [WGS84]	Latitude [WGS84]	Stratigraphic Unit	Reference
PV-2	1.83	0.03	-159.491	22.231	Koloa Volcanics	Garcia et al. 2010
KV03-4	1.83	0.03	-159.620	21.932	Koloa Volcanics	Garcia et al. 2010
KV04-10	1.97	0.04	-159.522	22.217	Koloa Volcanics	Garcia et al. 2010
KV03-2	1.99	0.06	-159.617	21.931	Koloa Volcanics	Garcia et al. 2010
KV05-16	2.1	0.04	-159.545	22.221	Koloa Volcanics	Garcia et al. 2010
0301-1	2.44	0.05	-159.589	21.952	Koloa Volcanics	Garcia et al. 2010
KV04-6	2.52	0.04	-159.461	22.167	Koloa Volcanics	Garcia et al. 2010
KV05-13	3.58	0.05	-159.459	22.062	Koloa Volcanics	Garcia et al. 2010
KV03-5	3.85	0.06	-159.588	21.953	Koloa Volcanics	Garcia et al. 2010
GA-566	3.87	0.04	-159.609	22.008	Koloa Volcanics	Garcia et al. 2010
GA-565	3.9	--	-159.642	22.535	Koloa Volcanics	Garcia et al. 2010
GA-650	3.92	0.03	-159.646	22.035	Koloa Volcanics	Garcia et al. 2010
KV05-10	3.92	0.06	-159.652	22.058	Koloa Volcanics	Garcia et al. 2010
KV04-21	4.14	0.2	-159.450	21.937	Koloa Volcanics	Garcia et al. 2010
KV04-19	4.3	0.11	-159.450	21.935	Koloa Volcanics	Garcia et al. 2010
KV04-16	4.31	0.17	-159.450	21.935	Koloa Volcanics	Garcia et al. 2010
KV05-7	4.35	0.13	-159.644	22.081	Koloa Volcanics	Garcia et al. 2010
KV04-17	4.36	0.18	-159.450	21.935	Koloa Volcanics	Garcia et al. 2010
KV05-17	4.43	0.24	-159.560	22.200	Koloa Volcanics	Garcia et al. 2010
KV04-24	4.46	0.25	-159.449	21.939	Koloa Volcanics	Garcia et al. 2010
KV04-22	4.51	0.07	-159.450	21.937	Koloa Volcanics	Garcia et al. 2010
KV05-9	4.57	0.08	-159.644	22.085	Koloa Volcanics	Garcia et al. 2010
KWQ-7H	0.375	0.004	-159.423	21.887	Koloa Volcanics	Hearty et al. 2005
GA642	1.46	0.07	-159.503	21.900	Koloa Volcanics	McDougall 1964
86KA4	3.91	0.03	-159.605	22.008	Makaweli member	Clague and Dalrymple 1988
86KA5	3.91	0.05	-159.605	22.008	Makaweli member	Clague and Dalrymple 1988
GA565	3.60	0.175	-159.640	22.045	Makaweli member	McDougall 1964
GA566	3.94	0.06	-159.605	22.006	Makaweli member	McDougall 1964
GA650	4.00	0.195	-159.643	22.032	Makaweli member	McDougall 1964
GA563	4.15	0.06	-159.647	22.028	Makaweli member	McDougall 1964
KA1213	3.43	--	-159.704	22.004	Napali Member	Evernden 1964
GA 561	4.63	0.07	-159.655	22.052	Napali Member	McDougall 1964
GA649	4.67	0.07	-159.654	22.052	Napali Member	McDougall 1964
GA564	5.77	0.28	-159.713	21.988	Napali Member	McDougall 1964
K19	3.81	0.06	-159.586	22.218	Napali Member	McDougall 1979
K18	3.93	0.1	-159.742	22.103	Napali Member	McDougall 1979
K21	4.03	0.06	-159.588	22.216	Napali Member	McDougall 1979
K17	4.24	0.09	-159.742	22.103	Napali Member	McDougall 1979
K15	4.42	0.16	-159.739	22.111	Napali Member	McDougall 1979
K16	4.45	0.11	-159.740	22.108	Napali Member	McDougall 1979
K3	4.51	0.08	-159.712	21.988	Napali Member	McDougall 1979
K7	4.53	0.1	-159.705	22.004	Napali Member	McDougall 1979
K9	4.71	0.11	-159.705	22.004	Napali Member	McDougall 1979
K2	4.90	0.09	-159.714	21.986	Napali Member	McDougall 1979
K10	5.05	0.16	-159.703	22.003	Napali Member	McDougall 1979
K1	5.07	0.13	-159.717	21.983	Napali Member	McDougall 1979
K6	5.14	0.2	-159.708	21.996	Napali Member	McDougall 1979
K22	4.27	0.11	-159.588	22.216	Napali Member dike	McDougall 1979
K20	4.36	0.24	-159.599	22.208	Napali Member dike	McDougall 1979
K4	5.13	0.06	-159.711	21.991	Napali Member dike	McDougall 1979
86KA6	3.95	0.05	-159.610	22.147	Olokele Member	Clague and Dalrymple 1988